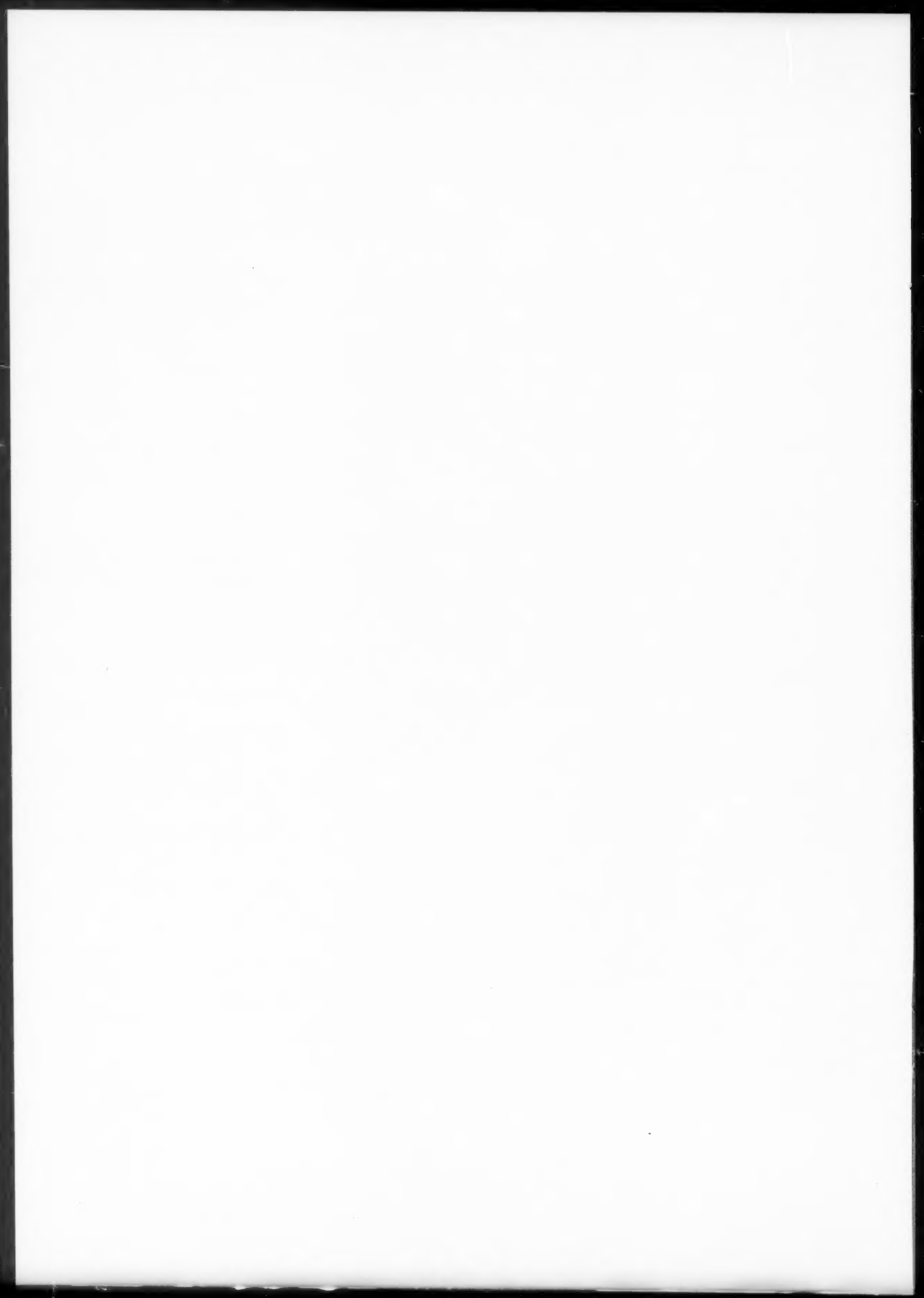


Author Index

- Abu El-Haija, A. J., 267
 Aernoudt, E., 115
 Ahn, D.-S., 273
 Al-Saleh, K. A., 267
 Allen, F. S., 247
 Anestiev, L. A., 281
 Arafah, D. E., 267
 Arnberg, L., 101
 Avni, R., 237
 Backmark, U., 101
 Bäckström, N., 101
 Barlat, F., 15
 Carlson, J. D., 187
 Cauwenberg, G., 115
 Chang, L., 125
 Chu, C. N., 303
 Chung, U.-I., 273
 Conrad, H., 187
 Cowie, J. G., 93
 Dannemann, K., 63
 Duquette, D. J., 63
 Fletcher, A. J., 247
 Gan, D., 73, 125
 Gibson, L. J., 37, 55
 Gomez, E., 225
 Grant, N. J., 225
 Guimaraes, J. R. C., 217
 Gurland, J., 151
 Halim, N. A., 267
 Ho, N. J., 145
 Hu, C. T., 167
 Inoue, A., 101
 Kamal, M. R., 267
 Kandil, K. M., 287
 Kao, P.-W., 73
 Karimi, A., 1
 Khalifeh, J. M., 267
 King, S., 247
 Kotkata, M. F., 287
 Landes, J. D., 137
 Lavernia, E. J., 225
 Lee, J.-Y., 273
 Lee, S., 167
 Leo, W. R., 1
 Li, J. C. M., 175
 Liaw, P. K., 137
 Lin, K. M., 167
 Mallik, A. K., 259
 Martz, P., L5
 Masumoto, T., 101
 Myers, M. R., 81
 Nabil Bassim, N., 199
 Needham, N. G., 81
 Oguchi, M., 101
 Padmanabham, R., 295
 Papirer, E., L5
 Pilkington, R., 81
 Reyes, S. J., L1
 Richmond, O., 15
 Russev, K. A., 281
 Sachdev, A. K., 31
 Saka, N., 303
 Saleh, N. S., 267
 Saxena, A., 137
 Shabel, B. S., 209
 Shea, M. M., 31
 Spalvins, T., 237
 Sprecher, A. F., 187
 Stoloff, N. S., 63
 Su, Y. L., 151
 Suh, N. P., 303
 Suriyayothin, N., 295
 Tjong, S. C., 145
 Triantafillou, T. C., 37, 55
 Tseng, T., 73
 Tuler, F. R., 93
 Unnikrishnan, K., 259
 Van Houtte, P., 115
 Varma, S. K., L1
 Vianco, P. T., 175
 Wu, L. T., 145



Subject Index

- Aging behaviour**
aging behaviour of a duplex stainless steel, 259
- Alloys**
analysis of the earing behaviour of aluminium
3004 alloys by means of a simple model based on yield loci calculated from orientation distribution functions, 115
effect of cold work on subgrain growth during recovery in Al-0.6Fe alloy, L1
negative creep in an amorphous metallic alloy, 175
simple procedure for calculating rockwell hardness conversion relationships for metallic alloys, 209
structures and properties of Mg-Al-Zr and Mg-Zn-Zr alloys produced by liquid dynamic compaction, 225
transmission electron microscopy study of fatigue deformation in Fe-25Cr-5Al alloy, 145
- Aluminium**
analysis of the earing behaviour of aluminium
3004 alloys by means of a simple model based on yield loci calculated from orientation distribution functions, 115
effect of cold work on subgrain growth during recovery in Al-0.6Fe alloy, L1
structures and properties of Mg-Al-Zr and Mg-Zn-Zr alloys produced by liquid dynamic compaction, 225
transmission electron microscopy study of fatigue deformation in Fe-25Cr-5Al alloy, 145
- Amorphous-crystalline selenium**
study of electrical conductivity of amorphous-crystalline selenium mixtures, 287
- Amorphous metallic alloy**
negative creep in an amorphous metallic alloy, 175
- Amorphous powders**
preparation of Fe-Cr-Mo-C amorphous powders and microstructure and mechanical properties of their hot-pressed products, 101
- Argon**
structures and properties of Mg-Al-Zr and Mg-Zn-Zr alloys produced by liquid dynamic compaction, 225
- Austenite**
twinning in metastable Fe-Ni-C austenite during elevated temperature deformation, 31
- Austenitic steel**
influence of waveform and long hold time on the corrosion fatigue crack growth behaviour of an austenitic steel, 137
- Autocatalysis**
initial nucleation sites, autocatalysis and the spread of the martensite burst in Fe-31.9Ni-0.02C, 217
- Ball milling**
ball milling of muscovite, L5
- Beams**
failure mode maps for foam core sandwich beams, 37
- Carbides**
effects of grain boundary carbides on low temperature impact properties of type 316 stainless steel, 73
effects of grain boundary carbides on the low cycle fatigue properties of type 316 stainless steel, 125
- Carbon**
effects of phosphorus on the hydrogen trapping at grain boundaries in low carbon steel, 273
initial nucleation sites, autocatalysis and the spread of the martensite burst in Fe-31.9Ni-0.02C, 217
preparation of Fe-Cr-Mo-C amorphous powders and microstructure and mechanical properties of their hot-pressed products, 101
twinning in metastable Fe-Ni-C austenite during elevated temperature deformation, 31
- Cavitation erosion rate**
phenomenological model for cavitation erosion rate computation, 1
- Cavity nucleation**
cavity nucleation and growth in a 1%Cr-0.5%Mo steel, 81
- Ceramics**
negative thermal expansion ceramics: A review, 303
- Chromium**
cavity nucleation and growth in a 1%Cr-0.5%Mo steel, 81
preparation of Fe-Cr-Mo-C amorphous powders and microstructure and mechanical properties of their hot-pressed products, 101
transmission electron microscopy study of fatigue deformation in Fe-25Cr-5Al alloy, 145
- Cold work**
effect of cold work on subgrain growth during recovery in Al-0.6Fe alloy, L1
- Compaction**
structures and properties of Mg-Al-Zr and Mg-Zn-Zr alloys produced by liquid dynamic compaction, 225
- Composites**
high temperature fatigue of three nickel-base eutectic composites, 63
- Corrosion**
influence of waveform and long hold time on the corrosion fatigue crack growth behaviour of an austenitic steel, 137
- Cracks**
comparison of the effects of dislocations around internal and surface cracks on fracture, 167

- Crack growth**
influence of waveform and long hold time on the corrosion fatigue crack growth behaviour of an austenitic steel, 137
- Creep**
negative creep in an amorphous metallic alloy, 175
- D.C. glow discharges**
structures and properties of Mg-Al-Zr and Mg-Zn-Zr alloys produced by liquid dynamic compaction, 225
- Deformation**
twinning in metastable Fe-Ni-C austenite during elevated temperature deformation, 31
- Dislocations**
comparison of the effects of dislocations around internal and surface cracks on fracture, 167
role of dislocations in the fracture of prestrained AISI 4340 steel, 199
- Earing behaviour**
analysis of the earing behaviour of aluminium 3004 alloys by means of a simple model based on yield loci calculated from orientation distribution functions, 115
- Electrical conductivity**
study of electrical conductivity of amorphous-crystalline selenium mixtures, 287
- Electrorheology**
electrorheology at small strains and strain rates of suspensions of silica particles in silicone oil, 187
- Elongation**
strain partition, uniform elongation and fracture strain in dual-phase steels, 151
- Erosion**
phenomenological model for cavitation erosion rate computation, 1
- Eutectic composites**
high temperature fatigue of three nickel-base eutectic composites, 63
- F.C.C. polycrystalline sheets**
prediction of tricomponent plane stress yield surfaces and associated flow and failure behaviour of strongly textured F.C.C. polycrystalline sheets, 15
- Failure**
failure mode maps for foam core sandwich beams, 37
prediction of tricomponent plane stress yield surfaces and associated flow and failure behaviour of strongly textured F.C.C. polycrystalline sheets, 15
- Fatigue**
effects of grain boundary carbides on the low cycle fatigue properties of type 316 stainless steel, 125
high temperature fatigue of three nickel-base eutectic composites, 63
influence of waveform and long hold time on the corrosion fatigue crack growth behaviour of an austenitic steel, 137
- Fatigue deformation**
transmission electron microscopy study of fatigue deformation in Fe-25Cr-5Al alloy, 145
- Flow**
prediction of tricomponent plane stress yield surfaces and associated flow and failure behaviour of strongly textured F.C.C. polycrystalline sheets, 15
- Flow localization**
flow localization models — A review, 93
- Fluid dynamics**
fluid dynamics of the formation of thin metal ribbons by rapid quenching from the melt, 281
- Foam core sandwich beams**
failure mode maps for foam core sandwich beams, 37
- Foam core sandwich panels**
minimum weight design of foam core sandwich panels for a given strength, 55
- Fracture**
comparison of the effects of dislocations around internal and surface cracks on fracture, 167
role of dislocations in the fracture of prestrained AISI 4340 steel, 199
- Fracture strain**
strain partition, uniform elongation and fracture strain in dual-phase steels, 151
- Grain boundaries**
effects of phosphorus on the hydrogen trapping at grain boundaries in low carbon steel, 273
- Grain boundary carbides**
effects of grain boundary carbides on low temperature impact properties of type 316 stainless steel, 73
effects of grain boundary carbides on the low cycle fatigue properties of type 316 stainless steel, 125
- High temperature fatigue**
high temperature fatigue of three nickel-base eutectic composites, 63
- Hydrogen**
effects of phosphorus on the hydrogen trapping at grain boundaries in low carbon steel, 273
structures and properties of Mg-Al-Zr and Mg-Zn-Zr alloys produced by liquid dynamic compaction, 225
- Impact**
effects of grain boundary carbides on low temperature impact properties of type 316 stainless steel, 73
- Iron**
effect of cold work on subgrain growth during recovery in Al-0.6Fe alloy, L1
initial nucleation sites, autocatalysis and the spread of the martensite burst in Fe-31.9Ni-0.02C, 217
preparation of Fe-Cr-Mo-C amorphous powders and microstructure and mechanical properties of their hot-pressed products, 101
transmission electron microscopy study of fatigue deformation in Fe-25Cr-5Al alloy, 145

- twinning in metastable Fe-Ni-C austenite during elevated temperature deformation, 31
- Lanthanum**
transmission electron microscopy investigations of second phases in the system (La, Sr)ZrO₃, 295
- Magnesium**
structures and properties of Mg-Al-Zr and Mg-Zn-Zr alloys produced by liquid dynamic compaction, 225
- Martensite burst**
initial nucleation sites, autocatalysis and the spread of the martensite burst in Fe-31.9Ni-0.02C, 217
- Mechanical properties**
preparation of Fe-Cr-Mo-C amorphous powders and microstructure and mechanical properties of their hot-pressed products, 101
- Metallic alloys**
simple procedure for calculating rockwell hardness conversion relationships for metallic alloys, 209
- Microstructure**
preparation of Fe-Cr-Mo-C amorphous powders and microstructure and mechanical properties of their hot-pressed products, 101
- Molybdenum**
cavity nucleation and growth in a 1%Cr-0.5% Mo steel, 81
preparation of Fe-Cr-Mo-C amorphous powders and microstructure and mechanical properties of their hot-pressed products, 101
- Muscovite**
ball milling of muscovite, L5
- Nickel**
high temperature fatigue of three nickel-base eutectic composites, 63
initial nucleation sites, autocatalysis and the spread of the martensite burst in Fe-31.9Ni-0.02C, 217
twinning in metastable Fe-Ni-C austenite during elevated temperature deformation, 31
- Nitriding mechanisms**
structures and properties of Mg-Al-Zr and Mg-Zn-Zr alloys produced by liquid dynamic compaction, 225
- Nitrogen**
structures and properties of Mg-Al-Zr and Mg-Zn-Zr alloys produced by liquid dynamic compaction, 225
- Nuclear techniques**
quantitative analysis of stainless steel using nuclear techniques, 267
- Nucleation**
initial nucleation sites, autocatalysis and the spread of the martensite burst in Fe-31.9Ni-0.02C, 217
- Orientation distribution functions**
analysis of the earing behaviour of aluminium 3004 alloys by means of a simple model based on yield loci calculated from orientation distribution functions, 115
- Oxygen**
transmission electron microscopy investigations of second phases in the system (La, Sr)ZrO₃, 295
- Panels**
minimum weight design of foam core sandwich panels for a given strength, 55
- Phosphorus**
the effects of phosphorus on the hydrogen trapping at grain boundaries in low carbon steel, 273
- Polyalkylene glycol**
quenching characteristics of polyalkylene glycol solutions in water, 247
- Quenching**
fluid dynamics of the formation of thin metal ribbons by rapid quenching from the melt, 281
quenching characteristics of polyalkylene glycol solutions in water, 247
- Rapid quenching**
fluid dynamics of the formation of thin metal ribbons by rapid quenching from the melt, 281
- Rockwell hardness**
simple procedure for calculating rockwell hardness conversion relationships for metallic alloys, 209
- Selenium**
study of electrical conductivity of amorphous-crystalline selenium mixtures, 287
- Silica**
electrorheology at small strains and strain rates of suspensions of silica particles in silicone oil, 187
- Silicon oil**
electrorheology at small strains and strain rates of suspensions of silica particles in silicone oil, 187
- Stainless steels**
aging behaviour of a duplex stainless steel, 259
effects of grain boundary carbides on low temperature impact properties of type 316 stainless steel, 73
effects of grain boundary carbides on the low cycle fatigue properties of type 316 stainless steel, 125
quantitative analysis of stainless steel using nuclear techniques, 267
- Steels**
effects of phosphorus on the hydrogen trapping at grain boundaries in low carbon steel, 273
influence of waveform and long hold time on the corrosion fatigue crack growth behaviour of an austenitic steel, 137
role of dislocations in the fracture of restrained AISI 4340 steel, 199
strain partition, uniform elongation and fracture strain in dual-phase steels, 151
- Strains**
electrorheology at small strains and strain rates of suspensions of silica particles in silicone oil, 187
- Strain partition**
strain partition, uniform elongation and fracture strain in dual-phase steels, 151

- Stress**
- prediction of tricomponent plane stress yield surfaces and associated flow and failure behaviour of strongly textured F.C.C. polycrystalline sheets, 15
- Strontium**
- transmission electron microscopy investigations of second phases in the system (La, Sr)ZrO₃, 295
- Subgrain growth**
- effect of cold work on subgrain growth during recovery in Al-0.6Fe alloy, L1
- Surfaces**
- prediction of tricomponent plane stress yield surfaces and associated flow and failure behaviour of strongly textured F.C.C. polycrystalline sheets, 15
- Thermal expansion ceramics**
- negative thermal expansion ceramics: A review, 303
- Thin metal ribbons**
- fluid dynamics of the formation of thin metal ribbons by rapid quenching from the melt, 281
- Transmission electron microscopy**
- transmission electron microscopy investigations of second phases in the system (La, Sr)ZrO₃, 295
 - transmission electron microscopy study of fatigue deformation in Fe-25Cr-5Al alloy, 145
- Tricomponent plane stress yield surfaces**
- prediction of tricomponent plane stress yield surfaces and associated flow and failure behaviour of strongly textured F.C.C. polycrystalline sheets, 15
- Twinning**
- twinning in metastable Fe-Ni-C austenite during elevated temperature deformation, 31
- Water**
- on the quenching characteristics of polyalkylene glycol solutions in water, 247
- Yield**
- analysis of the earing behaviour of aluminium 3004 alloys by means of a simple model based on yield loci calculated from orientation distribution functions, 115
- Zinc**
- structures and properties of Mg-Al-Zr and Mg-Zn-Zr alloys produced by liquid dynamic compaction, 225
- Zirconium**
- structures and properties of Mg-Al-Zr and Mg-Zn-Zr alloys produced by liquid dynamic compaction, 225
 - transmission electron microscopy investigations of second phases in the system (La, Sr)ZrO₃, 295

